Mechanical activation of mitochondrial energy metabolism during cell differentiation

Zong-Heng Wang[1], Christian Combs[1], Wenjing Zhao[1], Jay Knutson[1], Mary Lilly[2], and Hong Xu[1] *

Affiliations:

[1]National Heart, Lung, and Blood Institute, National Institutes of Health, Bethesda, MD 20892, USA

[2]National Institute of Child Health and Human Development, National Institutes of Health, Bethesda, MD 20892, USA

*Corresponding author. Email: Hong.Xu@nih.gov

Abstract:
In multicellular lives, differentiation of many types of stem and progenitor cells is often accompanied by a metabolic transition from glycolysis to mitochondrial oxidative phosphorylation. The mechanisms driving this metabolic transition in vivo are largely unknown. Here, we show that, during differentiation of the *Drosophila* female germline cyst, the surrounding somatic cells compress the cyst and increase the tension of cyst cells' membranes. Transmembrane channel-like, an evolutionarily conserved ion channel involved in mechanosensation, maintains cytosolic Ca^{2+} levels in compressed differentiating cysts. Cytosolic Ca^{2+} induces transcriptional activation of oxidative phosphorylation through a CaMKI-Fray-JNK signaling relay. Our findings demonstrate a molecular link between cell mechanics and mitochondrial energy metabolism, with implications in other developmentally orchestrated metabolic transitions in mammals.

One-Sentence Summary:
Mechanical forces from the surrounding tissue activate mitochondrial energy metabolism in differentiating cells in vivo.

Main Text:

Many types of stem cells and progenitor cells emphasize on glycolysis to preserve carbon sources for biosynthesis, while differentiated cells mainly rely on mitochondrial oxidative phosphorylation (OXPHOS), a more efficient way to produce ATP (*1, 2*). How mitochondrial energy metabolism is activated during cell differentiation in most developmental processes is unknown. Previous studies uncovered that OXPHOS is transcriptionally activated during differentiation of the *Drosophila* female germline cyst (Figure 1, A and B) (*3, 4*). In the *Drosophila* germarium, a cystoblast generated from asymmetric division of a germline stem cell undergoes 4 rounds of incomplete cytokinesis to form a cyst with 16 interconnected germ cells. Subsequently, the cyst is encased by somatic pre-follicle cells (pFCs), flattened into a one cell-thick disc, and starts to differentiate. The cyst that is consisted of an oocyte and fifteen nurse cells eventually becomes spherical in the budding egg chamber (Figure 1A) (*5-7*). The co-occurrence between OXPHOS activation and cyst shape remodeling intrigued us to test whether OXPHOS is induced in response to the flattening of differentiating cysts.

Differentiating cysts might be flattened by the surrounding pFCs. Notch (N) signaling controls a few pFCs, called cross-migrating cells (CMCs), to migrate centripetally and position themselves between cysts (fig. S1A) (*8*). To test whether impairing pFCs' migration could spare individual cysts from flattening, we inhibited N signaling in pFCs with an interfering RNA (RNAi) under the control of a pFC-Gal4 driver (109-30-Gal4) (*9*). The *N* RNAi disrupted pFCs' migration (fig. S1B), phenocopying *N* mutation (*8*). Importantly, most differentiating cysts were no longer separated by pFCs and became rounded rather than flattened, both in a sagittal view and in a three-dimensional (3D) reconstruction, although they appeared differentiating normally (Fig. 1, C-E, fig. S1, B and C, and Movies S1 and S2). The shape of earlier- or later-stage cysts was not affected. These results indicate that differentiating cysts are compressed by the surrounding pFCs.

A JNK-induced insulin-Myc feedforward loop activates the transcription of OXPHOS genes in differentiating cysts (*3*). When N signaling was inhibited in pFCs, both JNK and OXPHOS activities were downregulated in differentiating cysts (Fig. 1F, and fig. S1, D and E), examined by a JNK activity reporter (*puc*-nLacZ; Puc is a target and a negative regulator of JNK signaling) and a cytochrome c oxidase (COX) activity histochemistry, respectively (*3, 10*). Importantly, *puc* RNAi in germ cells that can ectopically activate JNK signaling partially restored COX activity in the background of *N* RNAi in somatic pFCs (Fig. 1F), suggesting that active N signaling in pFCs is essential for JNK-mediated OXPHOS activation in germ cells. Besides promoting CMCs' migration, N may also affect other aspects of interactions between pFCs and germ cells. We hence attempted to directly address whether pFCs' cross-migration is necessary for OXPHOS activation in differentiating cysts. In line with other cell migration models (*11, 12*), when wrapping around the cyst, CMCs formed protrusions that accumulated more F-actin than the CMC cell bodies did (Fig. 1, G-H). F-actin is also enriched in the pFCs between differentiating cysts (fig. S2, A and A'), presumably providing rigidity for pFCs to compress cysts. Chickadee (Chic), the fly homolog of profilin that facilitates actin polymerization, is highly expressed in pFCs (*13, 14*). When Chic is reduced in pFCs, pFC's positioning between cysts was impaired and differentiating cysts appeared partially relieved from compression, phenocopying the *N* RNAi (fig. S2B). Moreover, this genetic manipulation impaired

68 OXPHOS activation in differentiating cysts (Fig. 1I). By contrast, depleting Egalitarian (Egl), a key
69 regulator for cyst differentiation (*15*), barely affected OXPHOS in compressed cysts (fig. S3, A and B).
70 Taken together, our results demonstrate that compression by the surrounding pFCs activates OXPHOS in
71 differentiating cysts.
72
73 The fusome is a branched cytoskeleton-rich structure extending into all cyst cells through the actin-rich
74 intercellular bridges, ring canals (*16-18*). During cyst compression, the fusome may resist the sliding and
75 twisting between cyst cells and pull the membranes at the cyst cell interfaces, thereby locally stretching
76 their membranes (Fig. 2A). To test this idea, we performed fluorescence lifetime imaging microscopy on
77 living ovaries labelled with Flipper-TR, a cell membrane tension reporter (*19*). Increased membrane tension
78 enlarges the spaces between phospholipid tails and allows Flipper-TR to adopt a trans-conformation that
79 shortens its lifetime (*19*). As cysts differentiated, Flipper-TR lifetime became shorter at the cyst cells'
80 interfaces but remained the same at the cyst's borders. Relieving differentiating cysts from compression
81 with *N* RNAi in pFCs abolished the shortening of Flipper-TR lifetime at the cyst cells' interfaces (Fig. 2, B
82 and C, and fig. S4, A and B). Because cysts do not grow during differentiation (fig. S1F), cyst compression
83 is likely the driving force behind the expansion of cyst cells' interfaces.
84
85 Mechanoresponsive molecules on the cell membrane transduce mechanical stimuli to modulate various
86 cellular processes (*20-22*). To test whether any mechanoresponsive molecules is involved in OXPHOS
87 activation in differentiating cysts, we performed a candidate germline RNAi screen of 40 genes annotated
88 as "responsive to mechanical stimuli" for the phenotype of reduced COX activity (Table S1). RNAi against
89 transmembrane channel-like (Tmc) strongly impaired COX activity in differentiating cysts, as well as JNK
90 activation and Myc stabilization (Fig. 3A, and fig. S5). In the background of germline *Tmc* RNAi or tmc^1
91 mutation, germline *puc* RNAi restored most COX activity (Fig. 3B and fig. S5B). Tmc is an evolutionarily
92 conserved ion channel mediating mechanosensation in response to cell membrane expansion (*23, 24*),
93 suggesting that the expansion of cyst cell's membranes is sensed by Tmc and subsequently activates
94 OXPHOS through JNK.
95
96 The opening of Tmc channel allows the influx of Ca^{2+} into the cytosol (*25, 26*), prompting us to examine
97 the cytosolic Ca^{2+} profile along cyst development. We generated a UASz transgene that expresses a fusion
98 protein consisted of mTagBFP2 and GCaMP6s linked by a self-cleaving P2A peptide (fig. S6A). GCaMP6s
99 is a highly sensitive fluorescence Ca^{2+} reporter (*27*), while mTagBFP2 serves as the internal control to
100 normalize the expression levels of GCaMP6s (fig. S6B). We calibrated this ratiometric Ca^{2+} reporter in
101 perfused S2 cells using a series of Ca^{2+} buffers (fig. S6C). Simultaneous live imaging for both fluorescent
102 proteins in germaria revealed highly variable Ca^{2+} concentrations and distinct patterns of oscillations in
103 germ cells at different developmental stages (Fig. 3C). In the control germarium, undifferentiated cysts had
104 higher cytosolic Ca^{2+} levels (~239 nM) and Ca^{2+} oscillation frequency (5.8 times per 20 min), compared to
105 differentiating cysts (~123 nM and 1.5 times per 20 min) and budding egg chambers (69 nM and 0 time per
106 20 min) (Fig. 3, D and E, and Movie S3). *Tmc* RNAi had no obvious influence on either cytosolic Ca^{2+}
107 concentrations or oscillations in undifferentiated cysts, presumably due to high Ca^{2+} concentrations at this

stage (fig. S7, A and B, and Movies S4). In differentiating cysts, *Tmc* depletion lowered Ca^{2+} concentrations but increased Ca^{2+} oscillation frequency (Fig. 3F, fig. S7 A and C, and Movies S4). To further understand whether either or both of these two abnormalities may account for the OXPHOS defect in *Tmc* depleted differentiating cysts, we ectopically expressed a high-affinity Ca^{2+} binding Parvalbumin (PV) to sequestrate free intracellular Ca^{2+} (*28*). Compared to *Tmc* RNAi, PV expression led to a greater reduction in Ca^{2+} concentrations and diminished Ca^{2+} oscillations in differentiating cysts, while it similarly impaired JNK and COX activities (Fig. 3, B and F, fig. S7, fig. S8, A and B, and Movies S5). Also, the COX defect could be rescued by *puc* RNAi in both *Tmc* RNAi and PV expressing cysts (Fig. 3B). Therefore, the role of Tmc seems to maintain cytosolic Ca^{2+} concentrations that leads to OXPHOS activation through JNK, while the frequency of Ca^{2+} oscillations is not critical. As *Tmc* transcripts were uniformly expressed along cyst differentiation (fig. S9, A and B), other mechanisms must contribute to the higher basal Ca^{2+} levels in undifferentiated cysts. Although mitochondrial Ca^{2+} regulates cell metabolism (*29*), knockdown of the mitochondrial uniporter (MCU) had little impact on COX activity (fig. S8, C and D), further substantiating that cytosolic Ca^{2+} plays a critical role in mechanical activation of OXPHOS during cyst differentiation.

Despite high levels of cytosolic Ca^{2+}, JNK and OXPHOS are not activated in undifferentiated cysts. We therefore hypothesized that the signaling molecules, other than JNK (fig. S9, A and B), that function downstream of Ca^{2+} to activate OXPHOS in differentiating cysts might be absent in undifferentiated cysts. To this end, we assessed the potential involvement of a number of genes related to Ca^{2+} signaling and JNK pathway in OXPHOS activation in differentiating cysts (Table 2). Germline RNAi of Calcium/calmodulin-dependent protein kinase I (CaMKI) or Frayed (Fray), a conserved kinase regulating osmolarity (*30*), abolished JNK and COX activities in differentiating cysts. Moreover, COX activity in either *CaMKI* or *Fray* RNAi was partially restored by *puc* RNAi (Fig. 4A and fig. S10, A to D). Importantly, endogenous expression of GFP-tagged CaMKI was low in early cysts but markedly increased in differentiating cysts and thereafter, while the levels of endogenously expressed Fray-GFP remained nearly uniform (Fig. 4B and fig. S11A). Thus, the developmental patterns of CaMKI likely confine cytosolic Ca^{2+}-induced JNK activation to differentiating cysts.

To determine the epistasis between Fray and CaMKI, we generated a UASz transgene (UASz-Fray-3HA) expressing a wild-type, active Fray kinase (*31*). Overexpression of Fray enhanced both JNK and COX activities in differentiating cysts with *Tmc* or *CaMKI* RNAi, or overexpressing PV, and ectopically induced JNK activity in the budding egg chamber (Fig. 4, A and C, and fig. S11B). Therefore, Fray mediates Ca^{2+} and CaMKI in JNK and OXPHOS activation during cyst differentiation.

JNK-induced OXPHOS supports mtDNA replication during *Drosophila* oogenesis and maintains fertility (*3*). Consistent with our proposal that Tmc maintains cytosolic Ca^{2+} to activate JNK and OXPHOS, *Tmc* RNAi, *Fray* RNAi or PV overexpression markedly impaired mtDNA replication in the germline and caused reduced egg hatching rate (Fig. 4D and fig. S11, C and D).

147 Unicellular eukaryotes modulate energy metabolism directly in response to nutrient availability in the
148 environment, while stem cells and their differentiated progeny in multicellular organisms often reside in
149 the same environment with a controlled supply of nutrients (*32*). How OXPHOS activation is coupled with
150 cell differentiation remains an enigma. In this study, we uncover that mechanical forces from the
151 surrounding tissue function as developmental cues to activate mitochondrial energy metabolism during
152 differentiation of the *Drosophila* female germline cyst (Fig. 4E). During neuronal differentiation in the
153 mammalian cerebral cortex, differentiating neurons migrate towards the cortical plate by squeezing through
154 layers of cells while increasing their OXPHOS activity (*33, 34*). Moreover, maturing cardiomyocytes (CMs)
155 feature increased Ca^{2+}-dependent contractility and enhanced OXPHOS activity (*35, 36*). CM contraction is
156 modulated by stretch-activated ion channels and several CaMK genes are upregulated during CM
157 maturation (*37, 38*). Our work establishes a molecular link between cell mechanics and mitochondrial
158 energy metabolism, which may represent an evolutionarily conserved mechanism in animal development.

References and Notes:

1. X. Xu *et al.*, Mitochondrial regulation in pluripotent stem cells. *Cell Metab* **18**, 325-332 (2013).
2. N. Shyh-Chang, H. H. Ng, The metabolic programming of stem cells. *Genes Dev* **31**, 336-346 (2017).
3. Z. H. Wang, Y. Liu, V. Chaitankar, M. Pirooznia, H. Xu, Electron transport chain biogenesis activated by a JNK-insulin-Myc relay primes mitochondrial inheritance in Drosophila. *Elife* **8**, (2019).
4. Z. Chen *et al.*, Mitochondrial DNA segregation and replication restrict the transmission of detrimental mutation. *J Cell Biol* **219**, (2020).
5. K. Rust, T. Nystul, Signal transduction in the early Drosophila follicle stem cell lineage. *Curr Opin Insect Sci* **37**, 39-48 (2020).
6. J. R. Huynh, D. St Johnston, The origin of asymmetry: early polarisation of the Drosophila germline cyst and oocyte. *Curr Biol* **14**, R438-449 (2004).
7. M. de Cuevas, M. A. Lilly, A. C. Spradling, Germline cyst formation in Drosophila. *Annu Rev Genet* **31**, 405-428 (1997).
8. T. Nystul, A. Spradling, Regulation of epithelial stem cell replacement and follicle formation in the Drosophila ovary. *Genetics* **184**, 503-515 (2010).
9. T. R. Hartman *et al.*, Drosophila Boi limits Hedgehog levels to suppress follicle stem cell proliferation. *J Cell Biol* **191**, 943-952 (2010).
10. E. Martin-Blanco *et al.*, puckered encodes a phosphatase that mediates a feedback loop regulating JNK activity during dorsal closure in Drosophila. *Genes Dev* **12**, 557-570 (1998).
11. T. Svitkina, The Actin Cytoskeleton and Actin-Based Motility. *Cold Spring Harb Perspect Biol* **10**, (2018).
12. C. Le Clainche, M. F. Carlier, Regulation of actin assembly associated with protrusion and adhesion in cell migration. *Physiol Rev* **88**, 489-513 (2008).
13. R. Dominguez, K. C. Holmes, Actin structure and function. *Annu Rev Biophys* **40**, 169-186 (2011).
14. L. Cooley, E. Verheyen, K. Ayers, chickadee encodes a profilin required for intercellular cytoplasm transport during Drosophila oogenesis. *Cell* **69**, 173-184 (1992).
15. J. M. Mach, R. Lehmann, An Egalitarian-BicaudalD complex is essential for oocyte specification and axis determination in Drosophila. *Genes Dev* **11**, 423-435 (1997).
16. K. Roper, N. H. Brown, A spectraplakin is enriched on the fusome and organizes microtubules during oocyte specification in Drosophila. *Curr Biol* **14**, 99-110 (2004).
17. H. Lin, L. Yue, A. C. Spradling, The Drosophila fusome, a germline-specific organelle, contains membrane skeletal proteins and functions in cyst formation. *Development* **120**, 947-956 (1994).
18. N. C. Grieder, M. de Cuevas, A. C. Spradling, The fusome organizes the microtubule network during oocyte differentiation in Drosophila. *Development* **127**, 4253-4264 (2000).
19. A. Colom *et al.*, A fluorescent membrane tension probe. *Nat Chem* **10**, 1118-1125 (2018).
20. K. H. Vining, D. J. Mooney, Mechanical forces direct stem cell behaviour in development and regeneration. *Nat Rev Mol Cell Biol* **18**, 728-742 (2017).
21. S. van Helvert, C. Storm, P. Friedl, Mechanoreciprocity in cell migration. *Nat Cell Biol* **20**, 8-20 (2018).
22. Y. Chen, L. Ju, M. Rushdi, C. Ge, C. Zhu, Receptor-mediated cell mechanosensing. *Mol Biol Cell* **28**, 3134-3155 (2017).

199 23. P. Jin, L. Y. Jan, Y. N. Jan, Mechanosensitive Ion Channels: Structural Features Relevant to
200 Mechanotransduction Mechanisms. *Annu Rev Neurosci* **43**, 207-229 (2020).
201 24. C. D. Cox, N. Bavi, B. Martinac, Biophysical Principles of Ion-Channel-Mediated Mechanosensory
202 Transduction. *Cell Rep* **29**, 1-12 (2019).
203 25. Y. V. Zhang, T. J. Aikin, Z. Li, C. Montell, The Basis of Food Texture Sensation in Drosophila. *Neuron*
204 **91**, 863-877 (2016).
205 26. B. Pan *et al.*, TMC1 Forms the Pore of Mechanosensory Transduction Channels in Vertebrate Inner Ear
206 Hair Cells. *Neuron* **99**, 736-753 e736 (2018).
207 27. T. W. Chen *et al.*, Ultrasensitive fluorescent proteins for imaging neuronal activity. *Nature* **499**, 295-
208 300 (2013).
209 28. T. Pusl *et al.*, Epidermal growth factor-mediated activation of the ETS domain transcription factor Elk-
210 1 requires nuclear calcium. *J Biol Chem* **277**, 27517-27527 (2002).
211 29. A. Rossi, P. Pizzo, R. Filadi, Calcium, mitochondria and cell metabolism: A functional triangle in
212 bioenergetics. *Biochim Biophys Acta Mol Cell Res* **1866**, 1068-1078 (2019).
213 30. A. R. Rodan, A. Jenny, WNK Kinases in Development and Disease. *Curr Top Dev Biol* **123**, 1-47
214 (2017).
215 31. A. Sato, H. Shibuya, WNK signaling is involved in neural development via Lhx8/Awh expression. *PLoS*
216 *One* **8**, e55301 (2013).
217 32. M. G. Vander Heiden, L. C. Cantley, C. B. Thompson, Understanding the Warburg effect: the metabolic
218 requirements of cell proliferation. *Science* **324**, 1029-1033 (2009).
219 33. M. Knobloch, S. Jessberger, Metabolism and neurogenesis. *Curr Opin Neurobiol* **42**, 45-52 (2017).
220 34. M. Javier-Torrent, G. Zimmer-Bensch, L. Nguyen, Mechanical Forces Orchestrate Brain Development.
221 *Trends Neurosci* **44**, 110-121 (2021).
222 35. B. M. Ulmer *et al.*, Contractile Work Contributes to Maturation of Energy Metabolism in hiPSC-
223 Derived Cardiomyocytes. *Stem Cell Reports* **10**, 834-847 (2018).
224 36. E. Karbassi *et al.*, Cardiomyocyte maturation: advances in knowledge and implications for regenerative
225 medicine. *Nat Rev Cardiol* **17**, 341-359 (2020).
226 37. R. Peyronnet, J. M. Nerbonne, P. Kohl, Cardiac Mechano-Gated Ion Channels and Arrhythmias. *Circ*
227 *Res* **118**, 311-329 (2016).
228 38. T. Grancharova *et al.*, A comprehensive analysis of gene expression changes in a high replicate and
229 open-source dataset of differentiating hiPSC-derived cardiomyocytes. *Sci Rep* **11**, 15845 (2021).

230

Acknowledgements:
We thank F. Chanut for comments and editing on the manuscript; the Bloomington Drosophila Stock Center and the Vienna Drosophila Resource Center for providing fly lines; the Developmental Studies of Hybridoma Bank for various antibodies; Bestgene Inc. for Drosophila transgenesis service.

Fundings:
This work is supported by the National Heart Lung and Blood Institute Intramural Research Program and the Eunice Kennedy Shriver National Institute of Child Health and Human Development Intramural Research Program.

Author contributions:
Conceptualization: Z.-H.W., H.X.; Investigation: Z.-H.W., C.C.; Methodology: Z.-H.W., C.C., W.Z., J.K.; Funding acquisition: J.K., M.L., H.X.; Project administration: Z.-H.W., H.X.; Supervision: Z.-H.W., M.L., H.X.; Visualization: Z.-H.W., C.C., W.Z., H.X.; Writing - original draft: Z.-H.W., C.C., H.X.; Writing - review and editing: Z.-H.W., M.L., H.X.

Competing interests:
The authors declare no competing interests.

Data and materials availability:
All data are available in the main text or the supplementary materials. Materials are available upon request.

Figures and Legends:

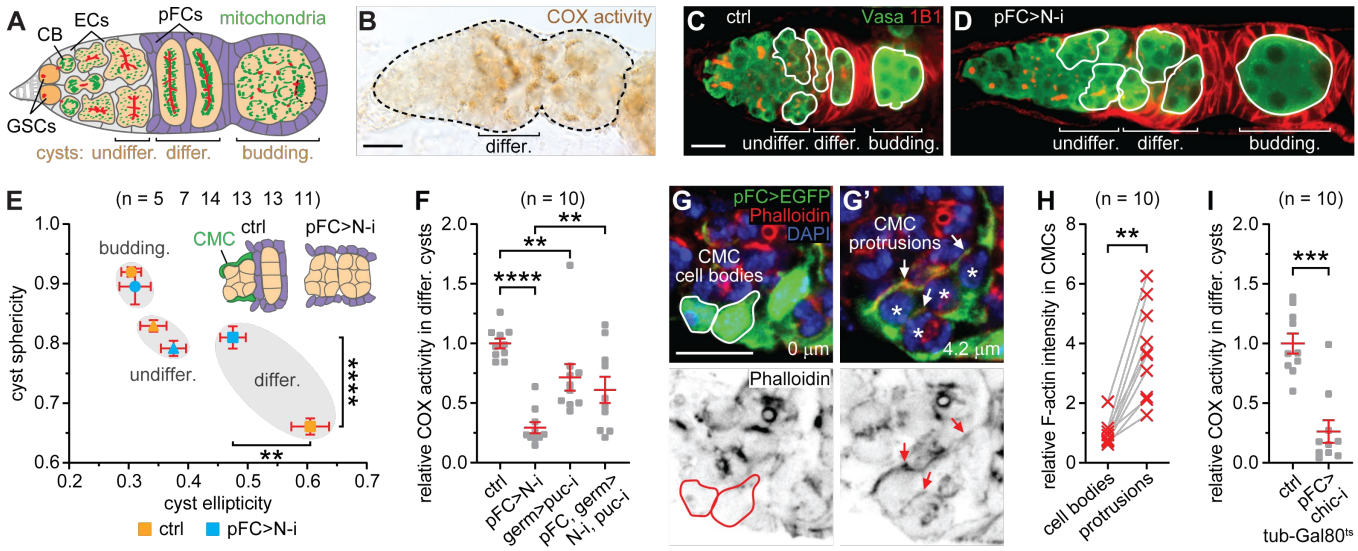

Figure 1. Cyst compression drives OXPHOS activation during differentiation.

(**A**) Schematic of the germarium. GSCs, germline stem cells. CB, cystoblast. ECs, escort cells. pFCs, pre-follicle cells. (**B**) COX activity in a germarium. (**C** and **D**) Germaria stained for Vasa (germ cells) and 1B1 (pFCs' cell membranes and fusomes). (**E**) Sphericity and ellipticity of developing cysts. CMC, cross-migrating pFC. (**F**) Quantification of COX activity in differentiating cysts. (**G** and **G'**) Two sections from a z-stack of CMCs in the germarium shown in fig. S2. Asterisks show germ cells in a cyst wrapped by CMCs. (**H**) Quantification of relative intensity of F-actin (Phalloidin) in 10 CMCs from 8 ctrl (control) germaria. (**I**) Quantification of COX activity in differentiating cysts. $^{**}P < 0.01$, $^{***}P < 0.001$, and $^{****}P < 0.0001$ [Mann-Witney tests for (E), (F), and (I); Wilcoxon signed-rank test for (H)]. Scale bars, 10 µm.

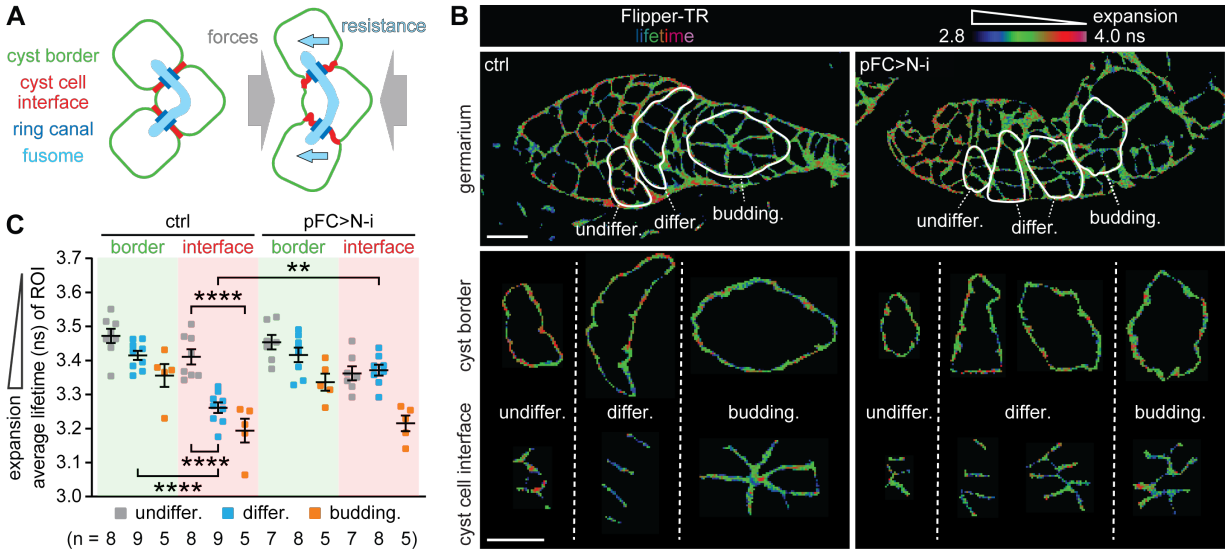

Figure 2. Cell membranes are expanded in compressed differentiating cysts.

(**A**) Cyst cells twist and slide relatively to each other during cyst compression. Resistance from the fusome may stretch membranes at the cyst cell interfaces. (**B**) Images of Flipper-TR lifetime at cell membranes in germaria. (**C**) Quantification of average Flipper-TR lifetimes in regions of interest (ROI). $^{**}P < 0.01$ and $^{****}P < 0.0001$ (Mann-Witney test). Scale bars, 10 µm.

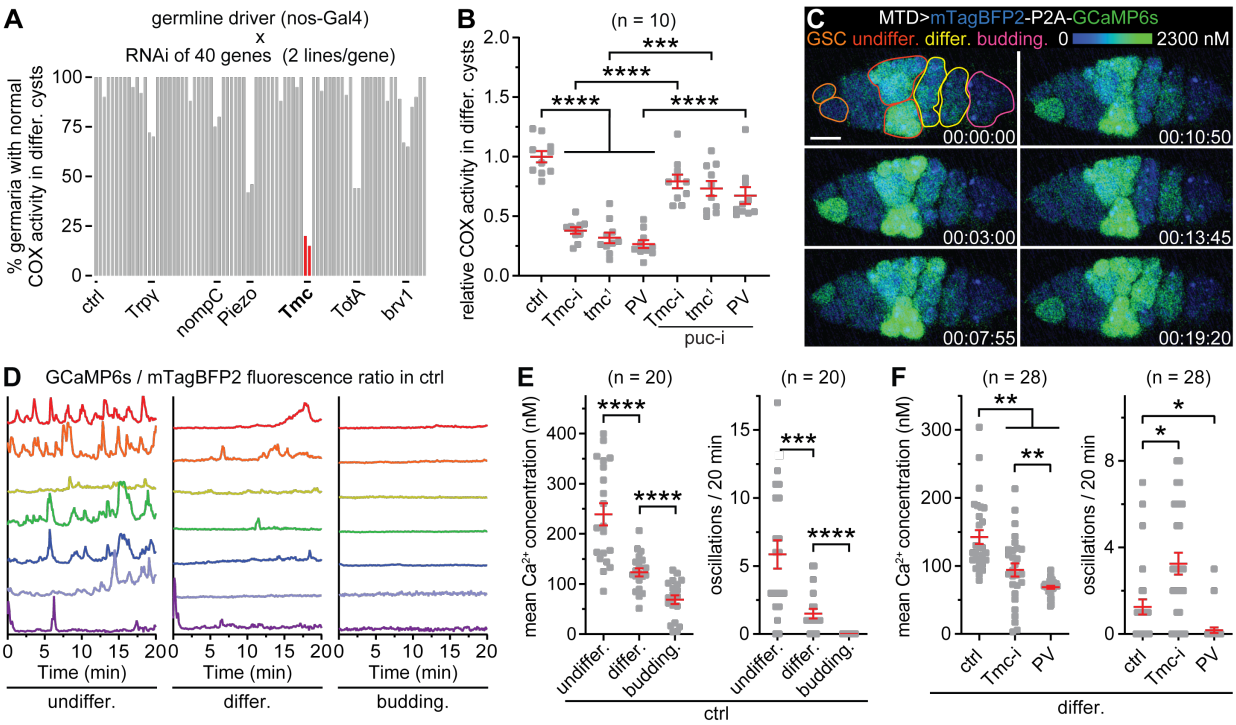

Figure 3: Tmc mediates OXPHOS activation by maintaining cytosolic Ca^{2+} concentrations.

(A) A germline RNAi screen for mechanoresponsive genes. (**B**) Quantification of COX activity in differentiating cysts. (**C**) Live recording showing Ca^{2+} levels and oscillations in germ cells at different stages (time stamp in h:min:s). The range for intracellular Ca^{2+} concentration is shown. (**D**) Representative traces of GCaMP6s/mTagBFP2 fluorescence ratio in individual ctrl germ cells at different developmental stages from 5 germaria. (**E** to **F**) Mean Ca^{2+} concentrations and Ca^{2+} oscillation frequency in individual germ cells from 5 germaria for (E) and 7 germaria for (F). $*P<0.05$, $**P<0.01$, $***P<0.001$, and $****P<0.0001$ [Kruskal-Wallis tests for the four groups in (B) and the three groups in (F, left); Mann-Witney tests between the two groups in (B), (E), (F), and (G)]. Scale bar, 10 µm.

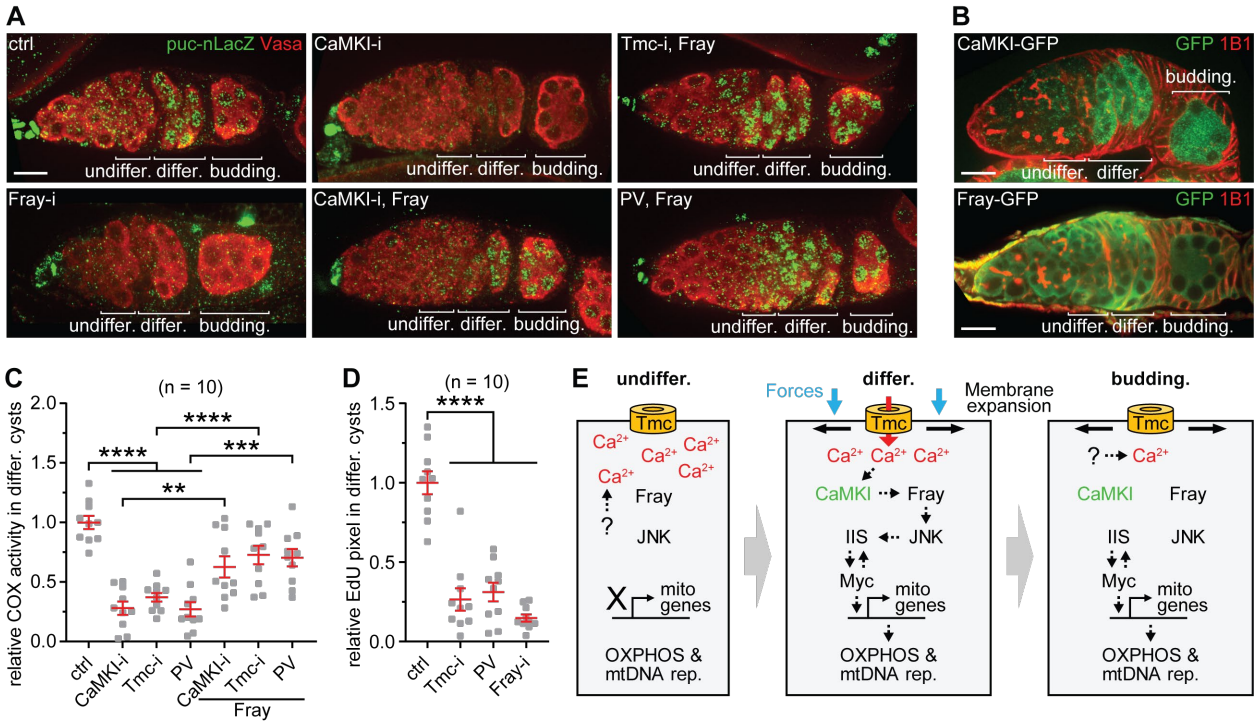

Figure 4: Cytosolic Ca^{2+} mediates mechanical activation of OXPHOS in differentiating cells through CaMKI and Fray.

(**A**) Visualization of JNK activity in germaria. (**B**) Expression of endogenous CaMKI-GFP and Fray-GFP in germaria. (**C**) Quantification of COX activity in differentiating cysts. (**D**) Quantification of EdU incorporated into mtDNA in differentiating cysts. (**E**) Schematic of the mechanotransduction pathway that activates OXPHOS during cyst differentiation. $^{**}P < 0.01$, $^{***}P < 0.001$, and $^{****}P < 0.0001$ [Kruskal-Wallis tests for the four groups in (C) and (D); Mann-Witney tests between the two groups in (C)]. Scale bars, 10 μm.

Supplementary Materials for

Mechanical activation of mitochondrial energy metabolism during cell differentiation

Zong-Heng Wang, Christian Combs, Jay Knutson, Mary Lilly, and Hong Xu

Corresponding author: Hong Xu, Hong.Xu@nih.gov

This PDF file includes:

Materials and Methods
Figs. S1 to S11
Tables S1 to S4
References (*1–8*)

Other Supplementary Materials for this manuscript include the following:

Movies S1 to S5

Materials and Methods

Fly stocks

Flies were maintained on standard BDSC cornmeal medium at 25°C. RNAi lines for candidate screen are listed in Tables S1 and S2. *Luciferase*-RNAi (ctrl, BL31603), *109-30*-Gal4 (soma-Gal4, BL7023), *nos*-Gal4 (germline, BL25751), *nos*-Gal4 (germline, BL32563), UAS-2xEGFP (BL6874), *tub*-Gal80^{ts} (BL7018), *MTD*-Gal4 (germline, BL31777), *puc*-nLacZ (*puc*-lacZ$^{A251.1F3}$, BL11173), NRE-EGFP (BL30728), *N*-RNAi (BL27988), *chic*-RNAi (BL34523), *tmc*^{1} (BL66556) (*1*), *puc*-RNAi (BL36085), *egl*-RNAi (BL43550), *MCU*-RNAi (BL67857), *CaMKI*-RNAi (BL35362), *CaMKI*-RNAi #2 (BL41900), *fray*-RNAi (BL42569), *fray*-RNAi #2 (BL55878), and Myc-GFP (BL81274) were obtained from the Bloomington Drosophila Stock Center. CaMKI-GFP (v318349) and Fray-GFP (v318460) were from the Vienna Drosophila Resource Center. Vasa-GFP (#109171) was purchased from the Kyoto *Drosophila* Genomics and Genetics Resources.

Female fly hatching rate

Virgin female flies with different genotypes were crossed with young (3-4 days) *w*^{1118} male flies in batches overnight. More than 180 embryos were collected and separated into 4 groups on grape juice agar plates with a small amount of yeast paste at the center. Plates were placed in a 25°C incubator for 2 days. The hatching rate was calculated as the number of hatched larvae divided by the number of embryos, averaged across the 4 groups.

Transgenic flies

To generate pUASz-mTagBFP2-P2A-GCaMP6s, GCaMP6s was amplified from pGP-CMV-GCaMP6s (#40753, addgene) and mTagBFP2 from pCAG-mTagBFP2 (*2, 3*). GCaMP6s and mTagBFP2, as well as a P2A fragments (GCCACCAACTTCTCCCTGCTGAAGCAGGCCGGCGACGTGGAGGAGAACCCCGGCCCC), were subcloned into XhoI-cut UASZ-1.0 (*4*) with the In-Fusion Cloning kit (Takara Bio Inc.). The PV DNA fragment and the coding region of Fray were amplified from pCMV-PV-GFP (#17301, addgene) and RE53265 (BDGP cDNA library), respectively. PV and Fray, as well as a C-terminal 3xHA tag, were subcloned into XhoI-cut UASZ-1.0 with the In-Fusion Cloning kit. Primers were listed in Table S3. Transgenic flies carrying these constructs were generated by Bestgene Inc.

Immunofluorescence staining and EdU labeling

Immunofluorescence staining and EdU labeling were performed as previously described (*5*). For immunofluorescence staining, antibodies/dye used were as follows: rabbit anti-Vasa (1:1000, Santa Cruz Biotechnology), rabbit anti-GFP (1:1,000, NB600-308, Novus Biologicals); mouse anti-Orb (1:800, 6H4, Developmental Studies Hybridoma Bank); mouse anti-Hts (1:800, 1B1, Developmental Studies Hybridoma Bank); mouse anti-β-galactosidase (1:1200, Z378A, Promega); Alexa Fluor 568-Phalloidin (1:500, A12380, Invitrogen); Alexa Fluor 568 donkey anti-rabbit IgG (1:600, A10042, Invitrogen), Alexa Fluor

568 goat anti-mouse IgG (1:600, A11004, Invitrogen), Alexa Fluor 488 goat anti-rabbit IgG (1:600, A11034, Invitrogen), and Alexa Fluor 488 goat anti-mouse IgG (1:600, R37120, Invitrogen).

The Click-iT EdU labeling kit (C10637, Invitrogen) was utilized to label EdU according to manufacturer's instructions. For EdU incorporation assay, ovaries were dissected in Schneider medium supplemented with 10% FBS (A3840002, Gibco) and pretreated with 7 μM aphidicolin (A0781, Sigma-Aldrich) in the medium for 3 h at room temperature. Then, the ovaries were incubated with 10 μM EdU and 7 μM aphidicolin in the medium with 10% FBS for 2 h. After three washes in the medium, ovaries were fixed in 4% PFA in PBS for 20 min, washed twice in PBS with 3% BSA for 5 min, and permeabilized in PBS with 0.5% Triton X-100 for 30 min. Subsequently, the ovaries were washed twice in PBS and co-stained with anti-1B1.

Samples were mounted with VECTASHIELD mounting medium with DAPI (H-1500, Vector Laboratories). Confocal images of germaria were collected on a Perkin Elmer Ultraview system (Zeiss Plan-apochromat 63×/1.4 oil lens, Volocity software, Hamamatsu Digital Camera C10600 ORCA-R2, Immersol immersion oil 518F) with a 0.3 μm step size. Images for morphological analysis of female germline cysts were acquired with an Instant Sim (iSIM) Super-Resolution Microscope (Olympus UPlanSApo 60×/1.30 Sil lens, Metamorph acquisition software, ORCA-Flash4.0 V2 Digital CMOS camera C11440, Silicone Immersion Oil SIL300CS-30SC) with a 0.2 μm step size. All confocal images were processed with NIH ImageJ (National Institutes of Health).

Morphological analysis of female germline cysts in 3D

Z-stack images were opened with Imaris (version 9.7, Oxford Instruments). Individual 16-cell cysts were identified based on DAPI staining. In germaria with somatic *N* RNAi, fused cysts were observed in some budding egg chambers. We only analyzed the shape of budding egg chamber cysts with 16 cells. In Imaris, 3D surface view of individual germline cyst was generated with the 'surfaces' tool. 'Draw' was used to manually trace the same cyst in each confocal step. After generating 3D surfaces with 'create surface', the values of cyst sphericity, ellipticity (oblate), and size were obtained in 'detailed statistics'. Images of 3D surfaces were generated with 'snapshot' and 3D movies were created with 'animation'.

Single molecule fluorescence in situ hybridization (smFISH)

Fluorescently (Quasar® 570) labeled Stellaris FISH probes against *Tmc*, and *JNK* mRNA were synthesized by Biosearch Technologies. smFISH on *Drosophila* ovaries were performed according to a published protocol (*6*). Briefly, dissected Vasa-GFP expressing ovaries were fixed in 4% PFA in PBS for 20 min. After 5×5 in washes with PBST (PBS and 0.2% Triton X-100), ovaries were permeabilized with 3 μg/ml proteinase K in PBS on ice for 1 h. Permeabilization was stopped by incubating ovaries in PBS with 20 mg/ml glycine and was followed by a post-fixation in PBST with 4% PFA for 20 min. After 5x2 min washes with PBST, ovaries were incubated in prehybridization solution (2× SSC and 10% formamide) at room temperature for 10 min. Prehybridization solution was removed, and 60 μl of hybridization solution (6 μl deionized formamide, 3 μg heparin, 1 μl salmon sperm DNA, 80 ng probe mix, 6 μg dextran sulfate, 120 μg BSA, and 5 μl of 20× SSC) was added. Ovaries were protected from light and incubated at 37°C

98 overnight. Ovaries were then washed for 2×15 min with prewarmed prehybridization solution in at 37°C,
99 followed by 2×5 min washes with PBS at room temperature. Z-stack images with smFISH, Vasa-GFP, and
100 nuclear (DAPI) channels were collected with the Perkin Elmer Ultraview system (Zeiss Plan-apochromat
101 63×/1.4 oil lens, Volocity software, Hamamatsu Digital Camera C10600 ORCA-R2, Immersol immersion
102 oil 518F) and processed with NIH ImageJ. The sequence of fluorescently labeled short DNA probes
103 targeting *Tmc* and *JNK* mRNA are listed in Table S4.
104
105 **Calcium imaging**
106 Three-day-old females were collected. Their ovaries were dissected in Schneider medium (Sigma-Aldrich)
107 and immerged in hydrogel as adapted from (*7*). Briefly, dissected ovaries were transferred into a droplet of
108 medium on a 22×22 mm coverslip that were previously coated with 3-(trimethoxysilyl) propyl methacrylate
109 (440159, Sigma Aldrich). Medium was then replaced by 15 µl of 10% PEG-DA hydrogel solution (GS700,
110 Advanced BioMatrix, Inc.) with 0.1% Irgacure 2959 (photo initiator, 410896, Sigma-Aldrich). A coverslip
111 treated with deperlent was placed above the hydrogel solution. The coverslip/coverslip sandwich was
112 illuminated by a UV light source for 30 s at 312 nm for gelation. The upper coverslip was removed. The
113 bottom coverslip with the hydrogel was placed into a Chamlide chamber (CM-S22-1, Quorum
114 Technologies) filled with Schneider medium. Time-lapse imaging (every 5 s for 20 min) of the middle
115 section (z-axis) of the germarium was performed on a Leica SP8 confocal microscope (HC PL APO CS2
116 63×/1.40 N.A. objective lens) using the Las X software (version 3.5.7). Fluorescence of GCaMP6s
117 (excitation: 488 nm, emission: 500-550 nm, and gain: 150%) and mTagBFP2 (excitation: 405 nm, emission
118 at 440-480 nm, and gain: 0%) were recorded simultaneously as videos at 8-bit depth.
119
120 The video flies were opened with NIH ImageJ. 'Freehand selections' was used to select germ cell areas.
121 Time-lapse fluorescence intensities for both channels in individual germ cells were obtained with 'plot z-
122 axis profile'. Time-lapse background intensities of each channel calculated from a 10×10 μm^2 square
123 outside the germarium were subtracted from the time-lapse fluorescence intensities. Time-lapse ratios of
124 GCaMP6s/mTagBFP2 intensities were imported into Origin 2021 (OriginLab Corporation). In Origin 2021,
125 Ca^{2+} oscillation in each germ cell during the 20-min recording were counted manually based on the
126 individual peaks of GCaMP6s/mTagBFP2 intensity ratio. In Excel, average Ca^{2+} level for each germ cell
127 was calculated by averaging the fluorescence ratio of the 20-min imaging. The amplitude of oscillation
128 spikes was calculated by subtracting the average ratio of two timepoints flanking the peak from the altitude
129 of the peak obtained in Origin 2021. The baseline Ca^{2+} level between oscillations was calculated by
130 averaging the ratio without the values of peaks.
131
132 For Ca^{2+} calibrations, the mTagBFP2-P2A-GCaMP6s fragment was firstly subcloned into the pIB/V5-His
133 vector (V802001, Invitrogen) with the In-Fusion Cloning kit. 2×10^6 S2 cells (*Drosophila* Genomics
134 Resource Center, S2-DRSC, from Nasser Rusan's lab) were seeded in a 60 mm dish and transfected with 2
135 µg the pIB-mTagBFP2-P2A-GCaMP6s-V5-His construct using Effectene Transfection Reagent (Qiagen).
136 After 2 days, cells were spread on concanavalin A-coated chambered coverglasses (155411, Thermo
137 Scientific) and permeabilized by 150 µM digitonin (D141, Sigma-Aldrich) in the zero free calcium buffer

138 (30 mM MOPS, pH 7.2, 100 mM KCl, 10 mM EGTA; see below) for 10 min. A series of buffers with 11
139 different free calcium concentrations were obtained by mixing the zero free calcium buffer (30 mM MOPS,
140 pH 7.2, 100 mM KCl, 10 mM EGTA) and the 39 μM free calcium buffer (30 mM MOPS, pH 7.2, 100 mM
141 KCl, 10 mM CaEGTA) in various ratios (Calcium Calibration Buffer Kit #1, Life Technologies) and added
142 to different wells of chambered coverglasses. Confocal images of transfected cells (n = 13~29 cells for each
143 calcium concentration) were acquired by a Leica SP8 confocal microscope (HC PL APO CS2 63x/1.40
144 N.A. objective lens) using the Las X software (version 3.5.7) with the same settings for Ca^{2+} imaging on
145 germaria. In Prism 9 (GraphPad), background removed ratios of GCaMP6s/mTagBFP2 intensities were
146 plotted to generate a sigmoidal standard curve that was then utilized to fit germ cell data.
147
148 **Membrane tension measurements**
149 Cell membrane tension was measured with Flipper-TR fluorescent tension probe (SC020, Cytoskeleton,
150 Inc.) (*8*). Dissected ovaries were incubated with 2 μM Flipper-TR in Schneider medium for 30 min. Single
151 z-plane FLIM images of the germarium regions were acquired using a Leica SP8 Falcon FLIM confocal
152 microscope, a HC PL APO CS2 63×/1.40 N.A. objective lens, and Leica Las X (version 3.5.7). Point
153 scanning excitation at a speed of 400 Hz was performed at 488 nm using a pulsed white-light laser operating
154 at 80 MHz with emission collected over a bandwidth of 550-650 nm onto a hybrid single molecule detector
155 (HyD SMD) at 16-bit digitization with a pinhole set to 1 A.U. Image size was set to 512×512 $pixels^2$ with
156 pixel sizes of 300 nm. Fluorescence from germaria as frame accumulated over 70 images to build up an
157 adequate number of photons per pixel for further analysis. Time-correlated single photon counting
158 histograms were collected with 136 channels in a 13 ns time window (97 ps per channel). Before lifetime
159 fitting, pixel binning of 2 was performed to provide peak counts of at least 600 photons/pixel for the dual
160 exponential fits, followed by a manual thresholding to omit background pixels. Fluorescence decay data
161 from full images was fitted to a dual exponential tail fit model in the Las X software. Images of the longest
162 lifetime were exported for further analysis. A custom program written in IDL (Interactive Data Language,
163 L3Harris Geospatial) was used to obtain average lifetime values in regions of interest (ROIs) from the
164 lifetime pixel-map images generated by the Las X software.
165
166 **COX activity histochemistry of fly ovaries**
167 Histochemical activity staining and quantification for cytochrome c oxidase (complex IV) were performed
168 according to the procedure from our previous study (*5*). Four to eight pairs of ovaries from 2~3 day-old
169 flies were dissected in PBS and ovarioles were separated by using a dissection needle. Ovaries were
170 incubated with COX staining solution [50 mM phosphate solution (pH 7.4), 4 mM 3,3'-diaminobenzidine,
171 2 μg/ml catalase, 200 μM cytochrome c, 4 mM antimycin A, 84 mM malonate, and 60 μM rotenone] for
172 30 min at room temperature. For negative control, ovaries (*Luciferase* RNAi) were treated with 2 mM KCN
173 in COX staining solution for 30 min at room temperature. Negative control was performed with each batch
174 of COX activity staining. All reactions were followed by 2×5 min washes with phosphate solution and 4%
175 paraformaldehyde fixation for 15 mins. After 2×5 min washes in phosphate solution, ovaries were immersed
176 in 80% glycerol in phosphate solution. Brightfield images of germaria were collected by a Zeiss Axio
177 Observer Z1 microscope (C-Apochromat 40×/1.1 W Corr objective lens for ovaries).

178
179 Relative ETC activities in differentiating cysts were quantified with ImageJ. From the opened images, areas
180 of differentiating cysts were isolated with 'freehand selections' and followed by 'clear outside'. The color
181 of the cysts was converted into gray and inverted to obtain images with black background. The COX
182 staining area was selected with 'color threshold'. Mean intensity of the selected COX staining area was
183 measured. Mean intensity of non-selected area was considered as background and subtracted from the mean
184 intensity of selected area. From each batch of activity staining, relative COX activity of ctrl differentiating
185 cysts was considered as '1', while the intensity from the negative control was considered as '0' activity.
186
187 **Quantification and statistical analysis**
188 Sample size was not predetermined by statistical methods. The experiments were not randomized.
189 Investigators were not blinded. Prism 9 (GraphPad) was used to plot data and perform statistical analyses.
190 Error bars in all charts represent standard errors. Mann-Whitney test (two-tailed) was used to determine the
191 mean differences between two unpaired groups, and Wilcoxon signed-rank test (two-tailed) for the
192 differences between two paired groups. Kruskal-Wallis test, followed by Dunn's multiple comparisons test,
193 was performed to compare three and more groups. Differences were considered statistically significant
194 when $P < 0.05$.

Supplementary Figures and Legends

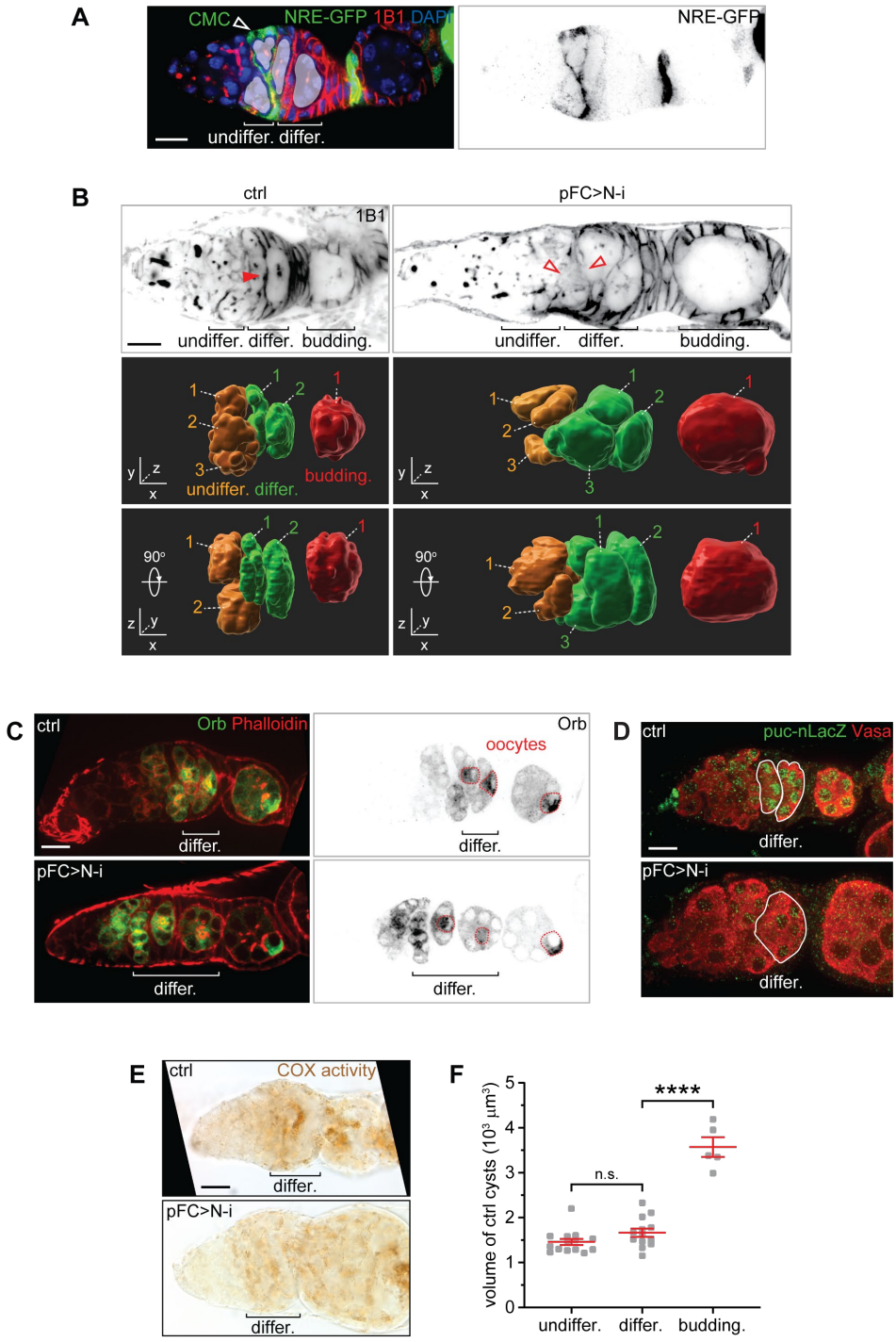

Fig. S1. pFCs' wrapping is required for compression and OXPHOS induction, but not differentiation, of the female germline cysts.

202 (**A**) Representative image of Notch signaling activity (NRE-GFP) in the germarium. CMC, cross-migrating
203 pFC. (**B**) 1B1 staining and three-dimensional reconstructions of the 16-cell cysts from Fig. 1, C and D. Red
204 Arrow head points to a pFC inserted between germline cysts. Hollow arrow heads indicate that pFCs are
205 absent between cysts. (**C**) Cyst differentiation visualized by Orb (oocyte marker) immunostaining. (**D**)
206 Visualization of JNK activity by *puc*-nLacZ in germaria. (**E**) Representative images of COX activity
207 histochemistry in differentiating cysts. (**F**) Cyst sizes in ctrl germaria. n = 14 (undifferentiated cysts), n =
208 13 (differentiating cysts), and n = 5 (budding egg chamber cysts) from 5 ctrl germaria. ****$P < 0.0001$ and
209 n.s., not significant (Mann-Witney test). Scale bars, 10 μm.

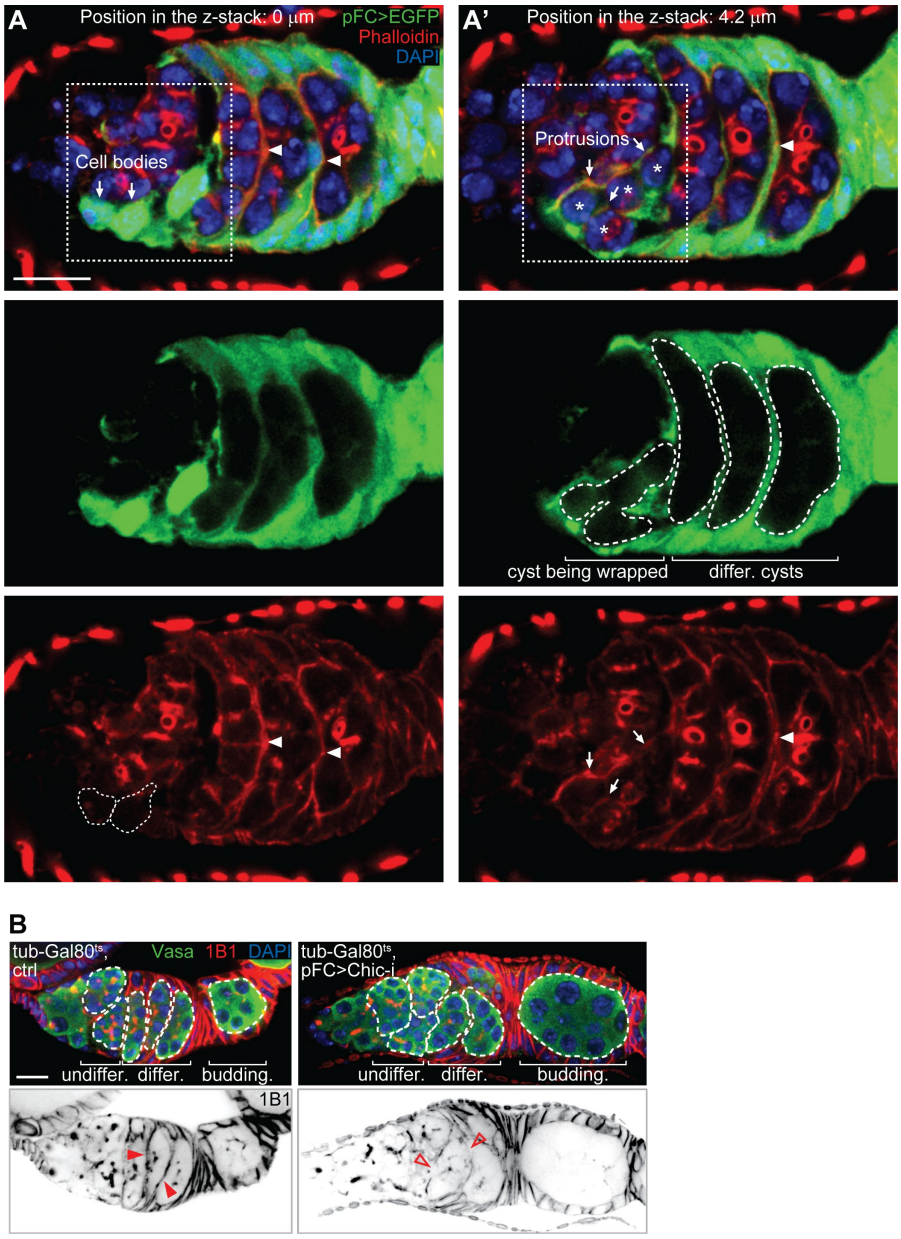

Fig. S2. F-actin in CMCs and the pFCs between differentiating cysts.

(**A** and **A'**) Representative images of a germarium expressing EGFP in pFCs. Arrows indicate CMC cell bodies or protrusions. Asterisks show the nuclei of cells in a cyst wrapped by CMCs. Arrowheads point to the pFCs between differentiating cysts. Germline cysts are outlined in the EGFP image, CMC cell bodies are outlined in the phalloidin image. (**B**) Germaria stained for Vasa, 1B1, and DAPI. Red arrow head points to pFCs inserted between germline cysts. Hollow arrow heads indicate that pFCs are absent between cysts. Scale bars, 10 µm.

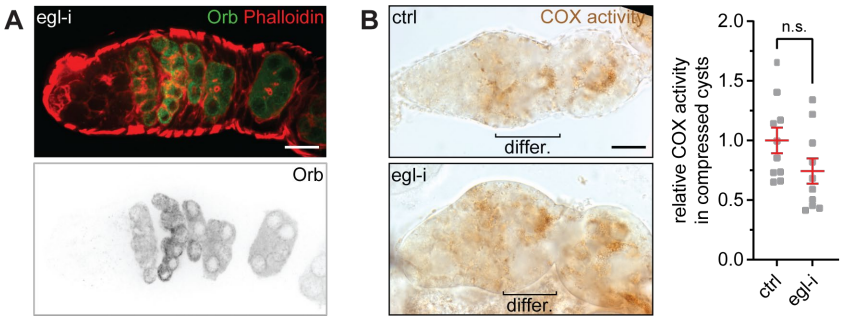

Fig. S3. OXPHOS induction is independent of cyst differentiation.

(**A**) Cyst differentiation is disrupted by *egl* RNAi. (**B**) COX activity in compressed cysts. n = 10 germaria for each genotype. n.s., not significant (Mann-Witney test). Scale bars, 10 µm.

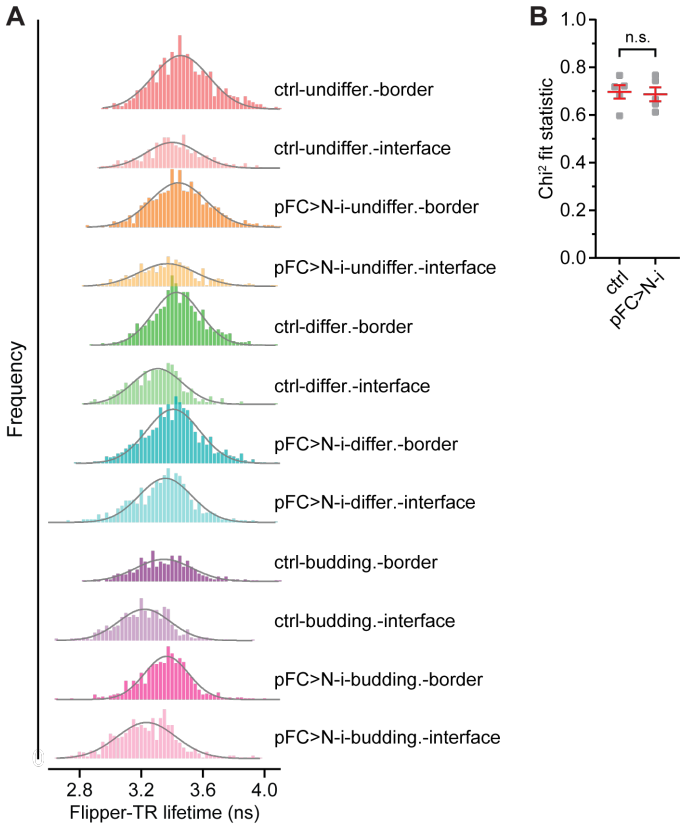

Fig. S4. Cell membranes are expanded in compressed differentiating cysts.

(**A**) Frequency distribution of Flipper-TR fluorescence lifetimes with Gaussian fits in ROIs. n = 8, 8, 7, 7, 9, 9, 8, 8, 5, 5, 5, 5 cysts, respectively. (**B**) Chi^2 measurements for goodness of fits for the single images of germaria stained with Flipper-TR membrane tension probe. n.s., not significant (Mann-Witney test).

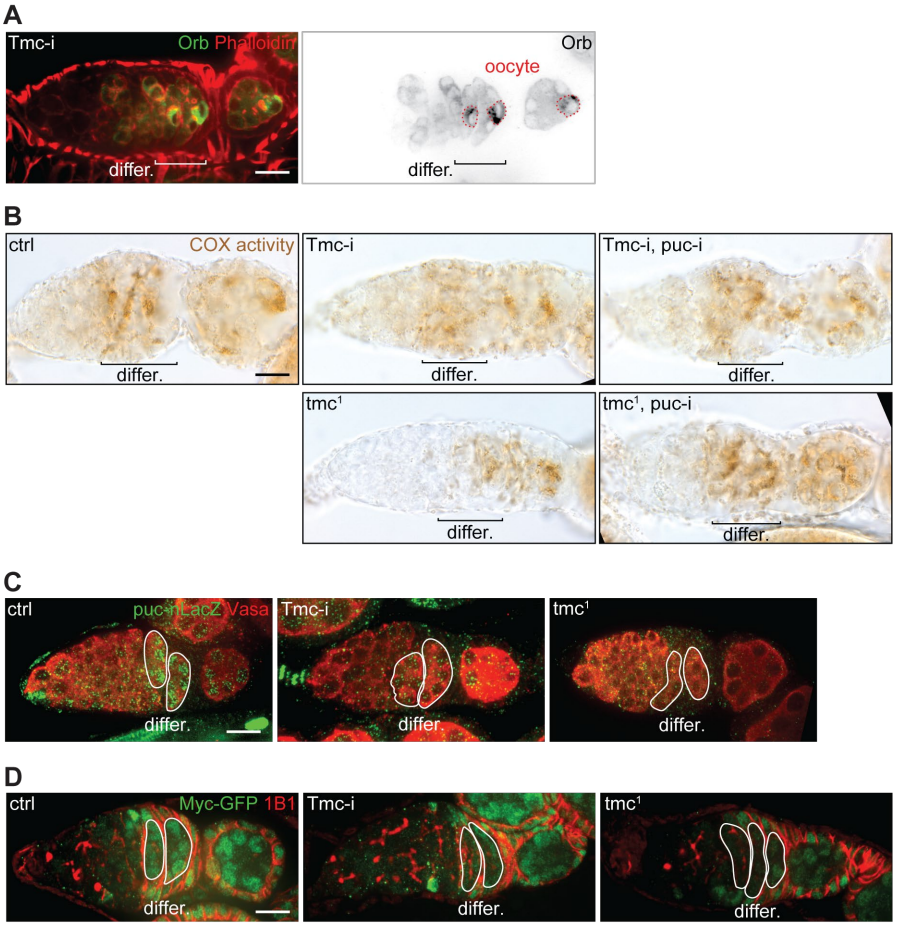

Fig. S5. OXPHOS induction in differentiating cysts requires Tmc.

(**A**) Cyst differentiation is normal in *Tmc* RNAi germarium. (**B**) COX activity histochemistry in germaria. (**C**) Representative images of JNK activity in germaria visualized by *puc*-nLacZ. (**D**) Representative images of endogenous Myc-GFP expression in germaria. Scale bars, 10 μm.

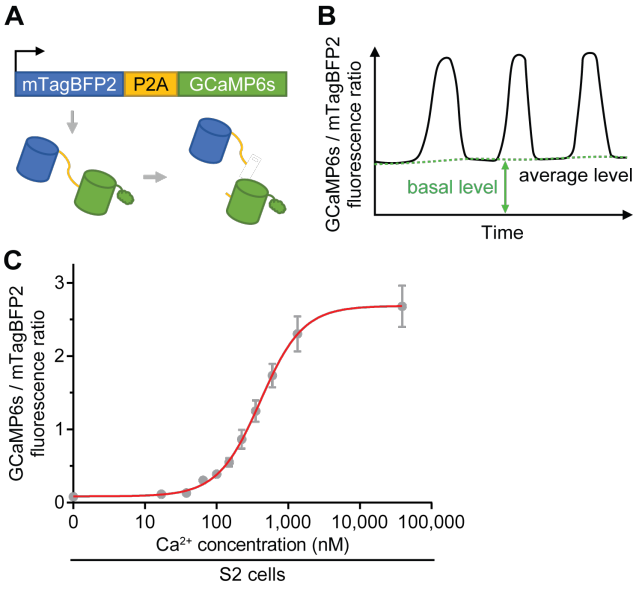

Fig. S6. The UASz-mTagBFP2-P2A-GCaMP6s fusion protein and its calibration in S2 cells.

(**A**) Schematic of UASz-mTagBFP2-P2A-GCaMP6s. (**B**) Ca^{2+} oscillation parameters. (**C**) Ca^{2+} calibrations of the mTagBFP2-P2A-GCaMP6s fusion protein in S2 cells. The standard curve is shown in red.

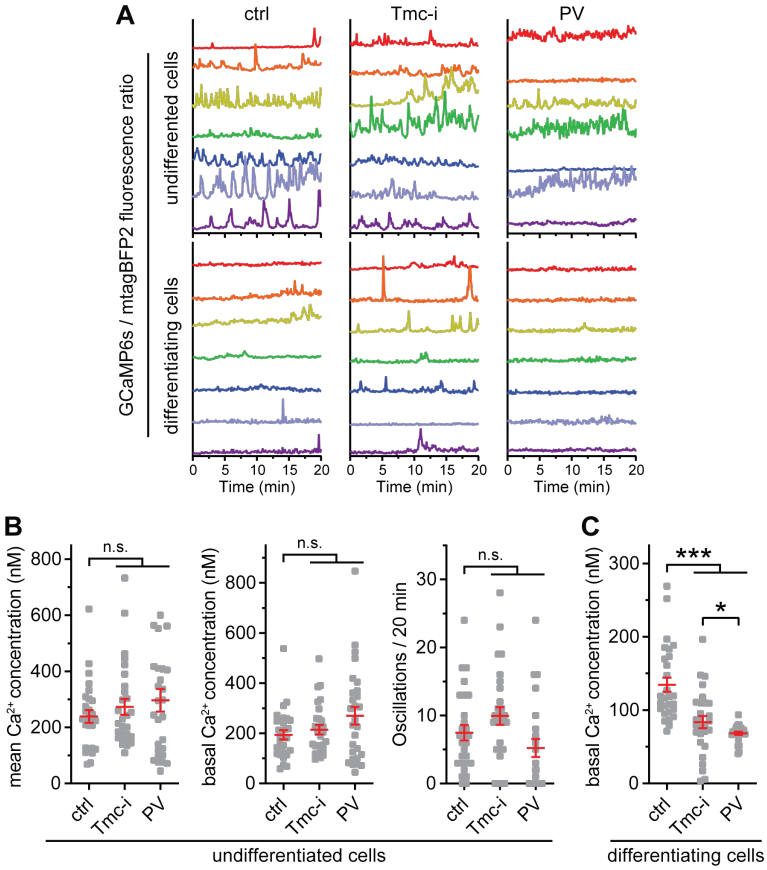

Fig. S7. Cytosolic Ca^{2+} in differentiating but not undifferentiated cysts can be manipulated by *Tmc* knockdown or PV expression.

(**A**) Representative traces of GCaMP6s/mTagBFP2 ratio in individual germ cells at different developmental stages. n = 7 germaria for each genotype. (**B** and **C**) Mean and basal Ca^{2+} concentrations, and Ca^{2+} oscillation frequency in individual germ cells. n = 28 cells from 7 germaria for each genotype. $*P < 0.05$, $***P < 0.001$, and n.s., not significant [Kruskal-Wallis tests for the three groups in (**B**) and (**C**); Mann-Witney tests between the two groups in (**C**)]. Scale bars, 10 μm.

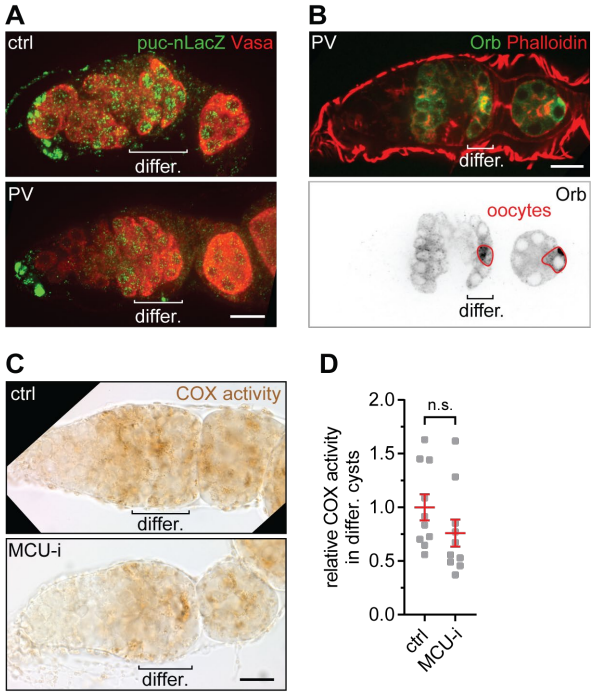

Fig. S8. Cytosolic but not mitochondrial Ca^{2+} is essential for JNK and OXPHOS induction in differentiating cysts.

(**A**) JNK activity is diminished in germ cells with expression of PV. (**B**) Cyst differentiation is normal when PV is expressed in the germline. (**C**) COX activity histochemistry in germaria. (**D**) Quantification of COX activity in differentiating cysts. n = 10 germaria for each genotype. n.s., not significant (Mann-Witney test). Scale bars, 10 μm.

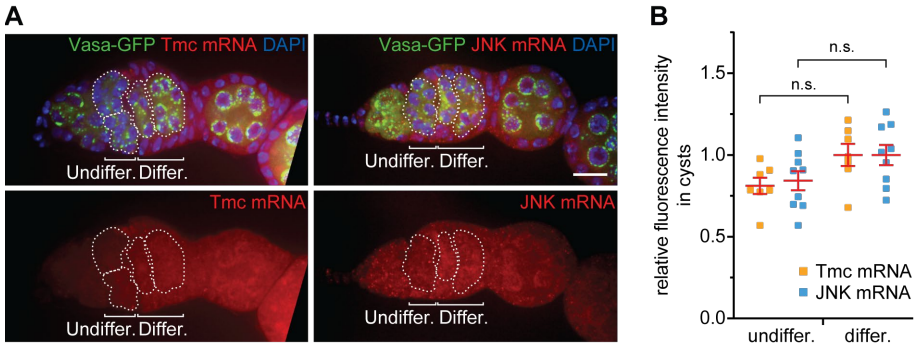

Fig. S9. Expression of *Tmc* and *JNK* mRNA in germaria.

(**A**) Visualization of *Tmc* and *JNK* mRNA in germaria by smFISH. (**B**) Quantification of *Tmc* (n = 7 germaria) and *JNK* mRNA (n = 9 germaria) in cysts. n.s., not significant (Mann-Witney tests). Scale bars, 10 μm.

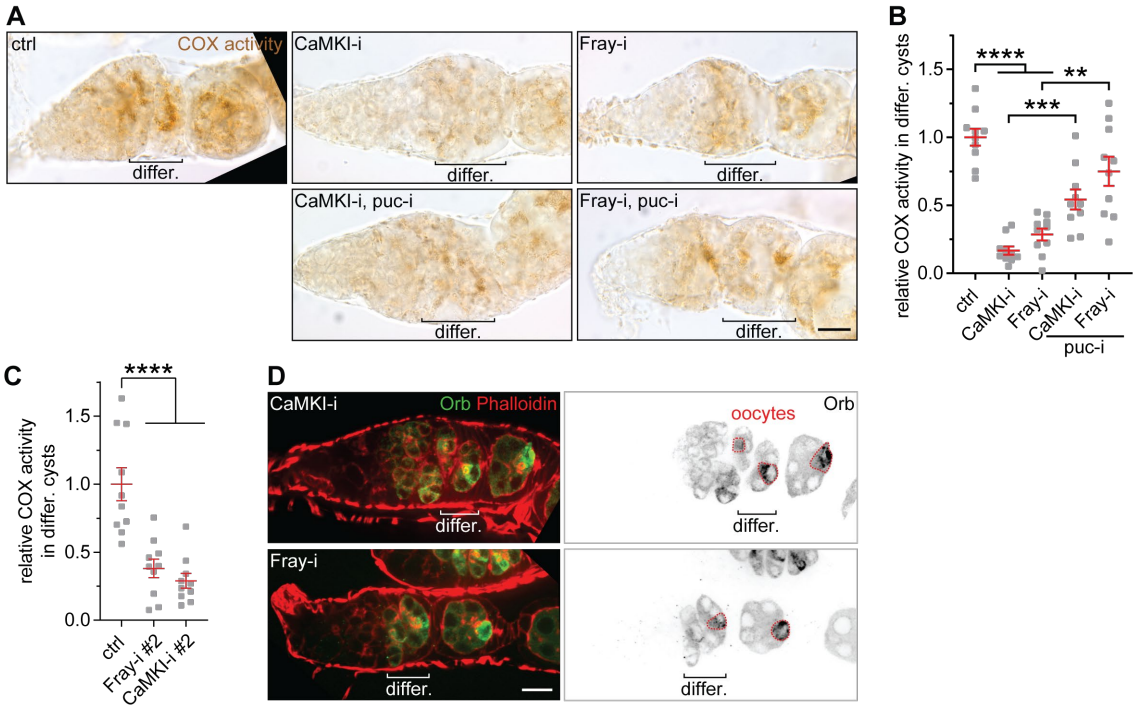

Fig. S10. CaMKI and Fray are required for OXPHOS induction in differentiating cysts.

(**A**) Representative images of COX activity histochemistry in germaria. (**B** and **C**) Quantification of COX activity in differentiating cysts. n = 10 germaria for each genotype. (**D**) Cyst differentiation is normal in *CaMKI* RNAi and *Fray* RNAi germaria. $^{**}P < 0.01$, $^{***}P < 0.001$, and $^{****}P < 0.0001$ [Kruskal-Wallis tests for (**B**) and (**C**); Mann-Witney tests for (**B**)]. Scale bars, 10 μm.

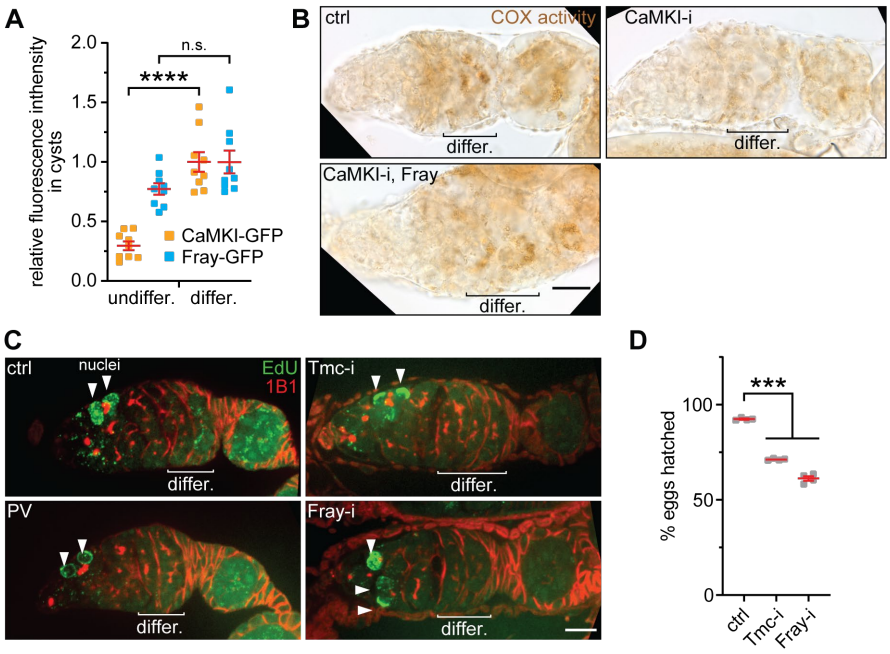

Fig. S11. Fray is downstream of CaMKI and the mechanotransduction pathway is required for mtDNA replication in the germline.

(**A**) Quantification for the expression levels of endogenous CaMKI-GFP and Fray-GFP in cysts. n = 10 germaria for each protein. (**B**) COX activity histochemistry in germaria. (**C**) mtDNA replication in germaria visualized with EdU incorporation. (**D**) Hatching rate of eggs laid by female flies with indicated germline RNAi. n > 180 eggs laid by 4 females for each genotype. ***$P < 0.001$, ****$P < 0.0001$, and n.s., not significant [Mann-Witney tests for (**A**); Kruskal-Wallis tests for (**D**)]. Scale bars, 10 μm.

291 **Supplementary Tables**

292

293 **Table S1. List of RNAi lines for the initial candidate screen used and the resulted COX activity.**

CG #	Genes	RNAi lines (BL: BDSC; v: VDRC)	% germaria with normal COX activity in differentiating cysts
	luciferase	BL31603	100
CG15148	beethoven	v19324	100
		v105152	90
CG7669	hemingway	v29201	100
		v108918	100
CG2171	Triose phosphate isomerase	BL26304	100
		BL51829	100
CG15427	turtle	BL54850	100
		v108746	100
CG17800	Down syndrome cell adhesion molecule 1	v25623	95
		v108835	100
CG6203	Fmr1	BL35200	92
		v110800	100
CG5996	Transient receptor potential cation channel γ	BL53313	72
		v105280	70
CG4536	inactive	v7126	100
		v100701	100
CG30092	jitterbug	v32433	100
		v102221	100
CG5594	kazachoc	v10278	100
		v101742	100
CG6706	metabotropic GABA-B receptor subtype 2	BL27699	100
		BL50608	100
CG33988	mid1	v30922	88
		v107431	100
CG5670	Na pump alpha subunit	v12330	100
		v100619	100
CG5842	nanchung	BL53312	100
		v100090	100
CG11020	no mechanoreceptor potential C	BL51722	75
		BL31689	80
CG15860	painless	BL51835	100
		v39477	100
CG9907	paralytic	v6131	100
		v104775	100
CG3478	pickpocket	v108683	100
		v330392	100
CG44122	piezo	v25780	42
		v105132	46
CG45783	Piezo-like	BL60501	100
		v109995	100
CG6504	Polycystic kidney disease 2	BL51502	100
		v110681	100
CG10537	Resistant to dieldrin	BL52903	100
		v100429	100

CG1058	ripped pocket	v8549	88
		v105463	100
CG6129	Rootletin	v22694	100
		v110171	100
CG1732	GABA transporter	v13359	95
		v106638	100
CG46121	Transmembrane channel-like	v39828	20
		v102145	15
CG8663	nervana 3	BL29431	100
		BL60367	100
CG14509	julius seizure	BL28764	93
		v4434	100
CG17150	dynein, axonemal, heavy chain 3	BL65239	100
		v35624	100
CG42685	CG42685	BL35005	100
		v49858	100
CG3525	easily shocked	BL38528	91
		v34286	100
CG31509	Turandot A	BL55378	44
		BL53244	44
CG6053	dynein, axonemal, intermediate chain 2	BL67961	100
		v35050	100
CG8546	pickpocket 26	BL25825	100
		v5110	100
CG14994	Glutamic acid decarboxylase 1	BL51794	100
		v32344	100
CG5751	Transient receptor potential cation channel A1	BL66905	88
		v37249	100
CG6963	gilgamesh	BL36719	100
		v26003	89
CG9472	brivido-1	BL31496	67
		v8424	65
CG16793	brivido-2	BL31670	85
		BL31671	90
CG13762	brivido-3	BL31385	100
		v101019	100

294

295 **Table S2. List of RNAi lines for Ca^{2+} signaling and JNK regulators, and the resulted COX activity.**

CG #	Genes	RNAi lines (BL: BDSC; v: VDRC)	% germaria with normal COX activity in differentiating cysts
	luciferase	BL31603	100
CG12530	Cdc42	BL35756	33
		v100794	69
CG8416	RhoA	v109420	69
		v12734	90
CG2248	Rac1	v49246	100
		BL34910	100
CG7177	Wnk kinase	BL42521	80
		BL62150	73
CG10295	p21-activated kinase	BL35141	55
		BL41714	61
CG2272	slipper	BL32948	87
		BL41605	100
CG4353	hemipterous	BL35210	100
CG9738	MAP kinase kinase 4	BL35143	85
CG7717	Mekk1	BL35402	100
CG8789	Wallenda	BL35369	100
CG9774	Rho kinase	BL35305	70
CG1495	CaMKI	BL35362	20
		v101380	20
CG18069	CaMKII	v100265	100
		BL35330	100
CG14992	Activated Cdc42 kinase	BL35264	100
CG7324	TBC1 domain family member 8/9	BL32929	100
CG14217	Tao	BL35147	100
CG1976	RhoGAP100F	BL32946	100
CG14895	Pak3	BL35373	80
CG18582	mushroom bodies tiny	BL35381	100
CG8114	pebble	BL36841	degeneration
CG16973	misshapen	BL42518	100
CG2849	Ras-like protein A	BL29580	55
		BL34375	50
CG11376	Zizimin-related	BL53946	91
CG7356	Transglutaminase	BL65086	100
CG10043	Rho-type guanine nucleotide exchange factor	BL32947	90
CG30115	Guanine nucleotide exchange factor in mesoderm	BL42545	90
CG45017	Inositol 1,4,5-triphosphate kinase 2	BL61831	100
CG17528	CG17528	BL42575	100
CG3086	MAP kinase activated protein-kinase-2	BL63717	75
CG17342	Lk6 kinase	BL60003	100
CG42349	Protein kinase C δ	BL28355	100
CG4527	Sterile20-like kinase	BL35179	70
CG5169	Germinal centre kinase III	BL41596	100
CG7693	frayed	BL42569	10
		BL41587	20

CG7097	happyhour	BL53699	100
CG4290	Salt-inducible kinase 2	BL55880	100
CG42856	Salt-inducible kinase 3	BL56941	100
CG4720	Apoptotic signal-regulating kinase 1	BL35331	92
CG18492	TGF-β activated kinase 1	BL53377	40
CG9842	Protein phosphatase 2B at 14D	BL40872	100
		BL25929	83
CG9819	Calcineurin A at 14F	BL58249	50
CG1455	Calcineurin A1	BL25850	90
CG4209	Calcineurin B	BL27307	100
CG11217	Calcineurin B2	BL38971	100
		BL27270	100

296

297 **Table S3. Primers for UASz cloning.**

Primer	Sequence
mTagBFP2-F	ATGGTGTCTAAGGGCGAAGAGC
mTagBFP2-P2A-R	GGGGCCGGGGTTCTCCTCCACGTCGCCGGCCTGCTTCAGCAGGGAGAAGTTG GTGGCGCCATTAAGCTTGTGCCCCAGTTTGCTA
GCaMP6s-F	GAGAACCCCGGCCCCATGGTCGACTCATCACGTCGTAAG
GCaMP6s-R	TCACTTCGCTGTCATCATTTGTACAAAC
PV-F	ATGGCCCAGGTGCAGCTGC
PV-3xHA-R	TTAAGCGTAATCTGGAACGTCATATGGATAGGATCCTGCATAGTCCGGGACG TCATAGGGATAGCCCGCATAGTCAGGAACATCGTATGGATAGCCTCCACCTG CGGCCGCGCTTTCGG
Fray-F	ATGACCTCCATACCCGCCAATC
Fray-3xHA-R	TTAAGCGTAATCTGGAACGTCATATGGATAGGATCCTGCATAGTCCGGGACG TCATAGGGATAGCCCGCATAGTCAGGAACATCGTATGGATAGCCTCCACCGT CCGTGATGGAGATCTGC

298

299 **Table S4. Fluorescently labeled short DNA probes for smFISH.**

	JNK-RB	TMC-RD 1	TMC-RD 2
1	TCGACGGTGTAGTGTTGGTG	TTTGTAGAATTCCCTCTTGG	CTAAGTCGTCTGAGTCTTTC
2	TGTGGATGGTGAAGTTGGTG	TTCAGTTCGTAGGATCTGTG	TAGTCGTGGTTCGATATCTC
3	TGGGCCGTAGATTAATGTAC	CTCTGGTTTTGCAATGGGAA	TGAATCAGTGGAACTCTCCG
4	GCATACTATTCCTTGGGCAC	GAAATTGTGTAGCTCTCCTC	TGTCGAAGGCATTGGTAGTG
5	GGGTGATAGTATCGTAAGCG	TGTCGTATAGACACTGGAGC	GTGGTGTATTCATCTTCTTC
6	GTTTCTTAATCGCCACATTT	CAGGCGGATGTTCTCAAAGA	CCACATAGTAGGGTCTATTC
7	ACATTTTGGAATGGTCGAGA	CGTGCCGCCATTAAAATTTT	TCTCCATCGTAGTAGATAGT
8	TATATGCTCGCTTGGCATGG	GGGAATGAGGACGGTAAGGA	ACACTCCTCCAGAAATTCAC
9	AGCTTCATTAGCTTGAATTC	GTGTGATTCGATTTCCTTGA	GCTGCCAAAAAAGTCATCGC
10	GCCAATTATGTTTTTATGGT	CATAAGCCATCGCAGGAATG	ACTTCCTTCAAACGCTTCTG
11	GCGGCGTAAAAGCATTAAGT	CAGCGGAATGGCAATCATGA	GTCGTCAGATTGGTTTGTAT
12	TGAAACTCTTCCAAGTTCCT	CTTTGTGGCAAAGTACTCGG	ACGATGACTTTGGAGAGCTC
13	CTCCATGACCAGGTAGACAT	AATATTTCAGGTATCCCTCG	CGCAGAAAGTCGATGCACAG
14	TGGCAGAGATTAGCGTCCAT	CCGGATGTGCTTGAATAGTA	GCACCAGTTTTGATTGACAT
15	ATCCAAGTCCATTTGGATGA	GGCGGTAAGGAAATAGGCTA	TACTGGGGAAAGGTCTTCTC
16	GCAAATAGGACATTCTGTCG	GCCACAAAGCTGTAGATGTA	TTCTCGGCTATCTTGAAGTC
17	ATTCCGCACAACATTTGATA	GGAAAGTTTTGAGTTGCGCG	CCCTGGTTATTAATCAACGT
18	TCCTGCTGAGTGTAAATGTT	GTGAAGAGCTTCCACGAGAA	AGAAGAATATGCCCATCCAC
19	ATGGCTTTAAGTCTCTGTGA	AGTTGCGATTATCCTTCTTT	CACTATCCACGAACGGAAGT
20	AGTCGGCCTTTACAACTATA	AGTATCCTCTGGAGTATGAC	GAAGTTGTTCGACTTGGAGG
21	GCCAGACCGAAATCCAAAAT	CTCAGAGTGATTAACCAGCA	ATGGTCAACAGCAGCGATAG
22	AAAGGTAGTTCCTGCAGTAC	CATGGGCAGGAAGAAGGAGA	GGGCAGGACACAAAGGAACA
23	TGACCACATAGGGAGTCATC	TCATAATGCGAGCCAATTGC	ATGAACTCAGCTATCCTGTT
24	TCTGGAGCCCTGTAATATCG	TGTTTGTTTCGTTCTCCAAT	GCAATGGAATCACAGTGCTC
25	TGTATCCCATGCCCAAAATG	CTCAGAGCCTCAATTGAACT	AGTTAGCGAAACCAGGTAGT
26	GACCATATGTCCACGTTCTC	TCCGAAGTACTTTCACCATA	CCTTAAAGATCTTCTTGCGC
27	GTATCATTTCGCCCATAATG	CAAGTTGCCGTTGATGTAGA	TACTCCTCCGTATCGAAATC
28	TTCCAGGAAACAGCACACCG	TGTAACACTTGAGACGCTGC	ATGCGTGAGATTAGCTCTTT
29	TTCCACTGATCTATATGATC	TGGTGTTGTCAGGTTGAGAA	AAACGAATCCTCATCCGACG
30	GGTGTACCTAATTGCTCAAT	GCAATGTGGTTGGCAAAGTT	GCAATCTGAACGATGTCCAC
31	CCGTTGCATAAACGAGGGTG	GTAATGTGGTGGGCAATGTG	GGGTCTCCTTTATGGGAAAA
32	TAGTTTCGGACGGTTGGCTG	CAATGTGGTAGGCAATGCTG	ATGTTTCTCCACTTTGAAGC
33	GTATCTAGGACGATTTTCCA	GGGCAATGTAGTAGGCAATG	TGTCCTTTTTATCCTTCATG
34	GTCTATCAAATGAGTATCCA	GTAGTTGTCGGAGATGTTTC	TTTGTATCCGGATCATGTTC
35	TTTGGAAACAAGCCATCGGG	TAACGTGGTCCAAGGTGATG	AACTGGCGCTGACAATTCTT
36	GGCGGCTATTCTGATTATTA	TTTATTTCGGCAGTGGTGAT	ATGTGGAATTTGCTTTTGGC
37	AGATTTCTAGCGTCAGAAGC	CAGGGGTTTTGTAGTATCTG	CGGGGGTTTTTTTTCATCAA
38	GCTCTGGATCAATGACTAGC	GTTGAGTTGGGTATTTCAGT	AAGGGTTTATCTTCCACTTC
39	AAAGCCTCGTCCACAGATAT	ATTGTGCTCAAAGTGGCAGA	CTTGAACTTGCCCAAACTTC
40	CACGTTGATATATTCATGCT	TCCGGTGGTGTAGATAAAGT	AAACTTGAACACCTCTGGCT
41	CCACTTCCTCAGCATCATAC	ATCACTGCCATAATCGTAGG	CTCGTTGTTTAGGTACTCTG
42	GTCCACGCTGTGATCATATG	CGACGGTTCCGAAGAGTAAT	AAAGCACAGACAATTGCCGC
43	CATAGATTAGCTCCTTCCAC	GCTTTCCTGTTCATCGAAAT	GTCCTTTTTGAGATTGACGG
44	TGCTTCGTAGTCCATGACTT	CTTCGTCTCATTTTCATCGA	AACTGGACACGCTGGACAAT
45	ACCGCGTTCTATTATTTGTA	CTGCTGTACTTGCTGGTAAA	AATGTAATAGGACCGGCTGT
46		CAATTAAATGGCCACCGACT	TCTGTGAATCCTGTCTCATA
47		GGTGTGGTTTGCCTAAAAGA	TGGGTATATTATCCGACCAA
48		TGGGAACTCTTCTTGTTGTG	CCTTATAATGTTGACCGTGG

300

301 **References:**

302 1. Y. V. Zhang, T. J. Aikin, Z. Li, C. Montell, The Basis of Food Texture Sensation in Drosophila.
303 *Neuron* **91**, 863-877 (2016).
304 2. T. W. Chen *et al.*, Ultrasensitive fluorescent proteins for imaging neuronal activity. *Nature* **499**, 295-
305 300 (2013).
306 3. H. Ochiai *et al.*, Genome-wide kinetic properties of transcriptional bursting in mouse embryonic stem
307 cells. *Sci Adv* **6**, eaaz6699 (2020).
308 4. S. Z. DeLuca, A. C. Spradling, Efficient Expression of Genes in the Drosophila Germline Using a
309 UAS Promoter Free of Interference by Hsp70 piRNAs. *Genetics* **209**, 381-387 (2018).
310 5. Z. H. Wang, Y. Liu, V. Chaitankar, M. Pirooznia, H. Xu, Electron transport chain biogenesis activated
311 by a JNK-insulin-Myc relay primes mitochondrial inheritance in Drosophila. *Elife* **8**, (2019).
312 6. T. Trcek, T. Lionnet, H. Shroff, R. Lehmann, mRNA quantification using single-molecule FISH in
313 Drosophila embryos. *Nat Protoc* **12**, 1326-1348 (2017).
314 7. S. Chanet, J. R. Huynh, Collective Cell Sorting Requires Contractile Cortical Waves in Germline
315 Cells. *Curr Biol* **30**, 4213-4226 e4214 (2020).
316 8. A. Colom *et al.*, A fluorescent membrane tension probe. *Nat Chem* **10**, 1118-1125 (2018).

317